Optimal Restoration of Active Distribution Systems with Voltage Control and Closed-Loop Operation

Renzo Vargas, *Member, IEEE*, Leonardo H. Macedo, *Member, IEEE*, Juan M. Home-Ortiz, José Roberto Sanches Mantovani, *Member, IEEE*, and Rubén Romero, *Senior Member, IEEE*

***Abstract*—This paper presents a new mixed-integer second-order cone programming model for solving the restoration problem in active distribution systems considering the optimal control of distributed generators (DGs), voltage regulators (VRs), on-load tap changers (OLTCs), and capacitor banks (CBs). In contrast to most of the works found in the literature, temporary loops may be formed in the network during the restorative operation state. This operating condition allows restoring the service to more loads. In this way, the objective function of the problem minimizes (i) the total load not supplied, (ii) the number of switching operations, (iii) the changes in the statuses of the voltage control devices and in the dispatch of the DGs, and (iv) the number of basic loops formed in the system. Several tests are carried out using a 53-node system for single-fault and multiple-fault scenarios. The results obtained with the proposed approach outperform the solutions achieved when only radial configurations are allowed in the problem. Moreover, it is also verified that the voltage control allows for more efficient restoration schemes.**

***Index Terms*—Distributed generation, distribution systems restoration, mixed-integer second-order cone programming, temporary closed-loop operation, voltage-dependent models.**

NOMENCLATURE

Indices:

i	Index for nodes
ij	Index for branches
k	Index for capacitor bank (CB) modules

Sets:

Γ_N	Set of nodes
Γ_N^{AS}	Set containing only the artificial substation node
Γ_N^{R}	Set of all real nodes
Γ_N^{D}	Set of demand nodes
Γ_N^{TS}	Set of subtransmission substation nodes
Γ_N^{CB}	Set of nodes with CBs
Γ_N^{DG}	Set of nodes with distributed generators (DGs)
$\Gamma_{\mathbb{S}}^{F}$	Set of sections under fault
Γ_B	Set of branches
Γ_B^{R}	Set of real branches
Γ_B^{DS}	Set of distribution substation branches
Γ_B^{C}, Γ_B^{O}	Set of real branches with the switch closed/open in the initial state of the system, not connected to a faulted section
Γ_B^{TC}	Set of branches with a voltage regulator (VR)/on-load tap changer (OLTC)

Parameters:

c_i^{LS}	Cost of the out-of-service load
c_{ij}^{SW}	Cost of line switching
c^{LP}	Cost of loop formation
c_i^{CB}	Cost of modifying the status of a CB
c_{ij}^{TC}	Cost of modifying the status of a VR/OLTC
c_i^{DGp}, c_i^{DGq}	Cost of changing the active/reactive output of a DG
$\mathbb{S}_i$	Section containing node i
R_{ij}, X_{ij}, Z_{ij}, B_{ij}^{SH}	Resistance/reactance/magnitude of the impedance/half of the line charging of a branch
$\overline{I}_{ij}$	Current capacity limit of a branch
V^N, $\underline{V}$, $\overline{V}$	Nominal/minimum/maximum voltage magnitudes
$\check{v}_i$	Estimate of the voltage magnitude
M_{ij}^V, M_{ij}^θ, M_i^P, M_i^Q	Big-M parameters
P_i^D, Q_i^D, S_i^D	Active/reactive/apparent demands
γ_i^Z, γ_i^I, γ_i^P	Participation factors of constant impedance/current/power loads of the active power demand
φ_i^Z, φ_i^I, φ_i^P	Participation factors of constant impedance/current/power loads of the reactive power demand
$\overline{S}_i^{DG}$	Apparent power capacity of a DG
$\underline{\sigma}_i$, $\overline{\sigma}_i$	Limit for capacitive/inductive power factors of a DG
N_i^{CB}	Number of CB modules
B_i^{CB}	Susceptance of a CB module
Λ_i^{CB}	Prefault state of a CB
Λ_{ij}^{TC}	Prefault state of a VR/OLTC
Λ_i^{DGp}, Λ_i^{DGq}	Prefault active/reactive generations of a DG
$\overline{\Delta}_{ij}^{TC}$	Regulation percentage of a VR/OLTC
$\overline{S}_{ij}^{DS}$	Apparent power capacity of a substation
N^{LP}	Number of basic loops allowed to be formed

Continuous variables:

$\hat{n}_i^{CB}$	Variation in the operation of a CB
$\hat{\delta}_{ij}^{TC}$	Variation in the operation of a VR/OLTC
$\hat{P}_i^{DG}$, $\hat{Q}_i^{DG}$	Active/reactive power variations of a DG
P_i^S, Q_i^S	Active/reactive power generations at a subtransmission substation
P_{ij}, Q_{ij}	Active/reactive power flows
I_{ij}^{SQ}	Square of the current magnitude
V_i, V_i^{SQ}	Voltage magnitude and its square value
θ_i	Voltage phase angle
ζ_{ij}, ξ_{ij}	Slack variables
P_i^{DG}, Q_i^{DG}	Active/reactive power generations of a DG
$\tilde{P}_i^D$, $\tilde{Q}_i^D$	Voltage-dependent active/reactive power demands
$\check{Q}_i^{CB}$	Total reactive power injection by a CB
δ_{ij}^{TC}	Auxiliary variable for a VR/OLTC
$Q_{i,k}^{CB}$	Reactive power injection by a CB module
f_{ij}^f, f_{ij}^e	Artificial flows

This work was supported by the Coordination for the Improvement of Higher Education Personnel (CAPES) – Finance Code 001, the Brazilian National Council for Scientific and Technological Development (CNPq), grants 305852/2017-5 and 305318/2016-0, and the São Paulo Research Foundation (FAPESP), under grants 2015/21972-6, 2018/20355-1, 2019/19632-3, 2019/01841-5, and 2019/23755-3.

The authors are with the Department of Electrical Engineering, São Paulo State University, Ilha Solteira, 15385-000, SP, Brazil (e-mail: renzo.vargas@unesp.br; leohfmp@ieee.org; juan.home@unesp.br; mant@dee.feis.unesp.br; ruben.romero@ unesp.br).

g_i^f, g_i^e	Artificial generations
z_{ij}	Auxiliary variable used in the linearization of $y_i y_j$
Binary variables:	
y_i	Status of the demand at a node
w_{ij}	Status of a switch
$h_{i,k}^{CB}$	Status of a CB module

I. Introduction

After the occurrence of a permanent fault in a distribution network, the continuous supply of electricity is interrupted not only to the section directly affected by the fault, which must be isolated for repair, but also to the sections downstream from the isolated section. This motivates distribution companies to take emergency actions, keeping as a main goal the reconnection of the largest number of out-service-loads in the least possible time. This goal is achieved by solving the service restoration problem in power distribution systems [1].

In a contingency scenario, the reconnection of loads is performed by reallocating out-of-service demand nodes to adjacent and auxiliary feeders through changing the status of the tie and sectionalizing switches. This reallocation is executed through network reconfiguration procedures, taking into account the operational and physical restrictions of the system. These restrictions include both of Kirchhoff's laws, voltage magnitude limits on nodes, current capacity on branches, power capacity of substations, and, conventionally, preserving the radial topology along the restoration process [2].

Even though distribution networks are planned with a weakly meshed topology, most of them are operated in radial configurations [3]. A radial operation topology presents technical advantages. For instance, it is possible to highlight the simplification of the coordination of the protective devices and the reduction of short-circuit current values in the network, reducing the basic levels of isolation of the devices installed in the network. Moreover, a weakly meshed structure allows reconfiguration procedures for technical loss reduction [4], the application of emergency restorative actions [5], and the execution of planned maintenance procedures [6]. On the other hand, the closed-loop operation topology has been considered to be an option for the radial operation in normal state [4] and as a temporary arrangement for load transfer [7], in order to avoid in-service customers experiencing short-term interruptions and long-term voltage dips. The advantages of a permanent closed-loop operation topology include lower costs associated with technical losses [4] and reliability improvement [8]. In contrast to [8], in this work, temporary closed-loop operation topologies are allowed as a strategy to improve the system capacity in the restorative state, which consists of the period of time between the fault isolation and the repair of the section with the permanent fault.

The penetration of distributed generators (DGs) in distribution systems has been increasing significantly in recent times. In normal operation, these devices can supply load locally, reducing congestion during peak load times and providing dynamic regulation of the voltage profile [9]. During fault events, DGs can alleviate the power flows on some lines of the network, allowing for more load to be reconnected to the system [10]. However, the DGs connected to the network also bring challenges to the operation of distribution systems, since reverse power flows, which lead to voltage rises, may occur when these devices inject high levels of power to the system [9].

Voltage control devices, such as voltage regulators (VRs), power transformers with on-load tap changers (OLTCs), and capacitor banks (CBs), provide benefits to the operation of distribution systems under heavy load conditions, improving the voltage profile, minimizing the technical losses, and correcting the power factors of the loads [3]. Besides that, these devices facilitate the operation of DGs [11]. In modern distribution networks, the centralized control, based on information and communication technologies, allows for an optimal and coordinated adjustment of such devices, providing flexibility for the system operation [12], [13]. The control of these devices can be considered in the service restoration for increasing the amount of load restored, providing better solutions for the problem [14].

Several heuristic and metaheuristic algorithms have been proposed to solve the restoration problem in distribution systems [15]–[18]. These approaches can provide solutions in adequate computational times, but cannot ensure optimality [19]. Another approach to solve an optimization problem consists of using exact methods to solve the mathematical modeling of the problem directly. In this context, [20] presents a complete and general model for the service restoration problem in passive distribution networks, including constraints that ensure the radiality of the system, allowing that some sections of the network can be de-energized so that other sections can be reconnected.

The traditional action for service restoration in passive distribution systems, therefore, consists of performing the minimum number of switching operations in order to change the topology of the network, maintaining radiality, with the objective of reconnecting the maximum amount of load disconnected due to a fault. In modern active distribution systems, the centralized control of the devices present in the network allows for more flexible restoration schemes that include actions such as reconfiguration, adjustment of voltage control devices, temporary closed-loop arrangements, and DG redispatch, so that the restoration process can be more effective, allowing more load to be reconnected. In this topic, reference [5] presents a tabu-search-based algorithm for the service restoration problem of radial distribution systems, considering the simultaneous control of DGs, VRs, and CBs. Reference [10] presents a mixed-integer second-order cone programming (MISOCP) formulation for the restoration problem of radial distribution systems, considering the presence of DGs that can only operate when connected to the main network. Reference [14] presents an MISOCP model for the restoration of radial distribution systems considering voltage regulation devices and distributed generation. The authors consider partial restoration solutions, in which some sections of the network remain de-energized so that other sections can be re-energized, as presented in [20].

Other works have presented mathematical models to solve the restoration problem after severe fault events in distribution networks, considering microgrid formation with DGs, without the possibility of load transfer among adjacent feeders [21], [22]. Also, in the context of the service restoration problem after

severe fault events, reference [23] presents a mixed-integer linear programming formulation for the problem of microgrid formation, which considers a meshed operation of the network, with islanded DGs.

The main contribution of this work is a new MISOCP model for the problem of service restoration in active distribution systems, considering network reconfiguration; DG redispatch; and voltage control through the optimal adjustment of substations' OLTCs, VRs, and CBs, together with the strategy of allowing the formation of temporary loops in the network during the restorative state, with total control on the number of formed loops. The results indicate that the proposed approach allows more load to be restored, both in single-fault and multiple-fault scenarios, than by considering the conventional restoration strategy that only allows radial topologies without considering voltage control.

In relation to the existing works available in the literature that present models for the restoration problem, the proposed model has the following contributions:

1. Proposal of a new philosophy for the operation of radial distribution networks in the restorative state, enabling the temporary closed-loop operation to add flexibility to the restoration process;
2. A precise voltage-dependent formulation to represent the operation of CBs;
3. A new set of constraints for modeling substations' OLTCs and VRs that present a good trade-off between precision and complexity;
4. A set of constraints that provides full control on the network topology, allowing to determine the optimal topology of the network operation in the restorative state.

This work is structured as follows: Section II presents the proposed MISOCP formulation for the problem of optimal restoration of distribution networks with voltage control, DG redispatch, and temporary closed-loop operation; Section III presents the results and discussion for single-fault and multiple-fault scenarios, considering the possibility of temporary closed-loop operation of the system with and without voltage control; and Section IV presents the conclusions of the work.

II. Mathematical Model for the Problem

In this section, the mathematical formulation proposed to solve the problem of optimal restoration of distribution systems is presented as an MISOCP model.

A. Objective function

The objective function $\mathcal{F}$, presented in (1), minimizes the nonrestored demand, penalizes changes in the operating states of the switches, CBs, DGs, OLTCs, and VRs, while reducing the number of basic loops (the definition of a basic loop can be found in [24]) formed in the network.

$$\begin{aligned}\text{minimize}\,\mathcal{F} = &\sum_{i\in\Gamma_N^D|\mathbb{S}_i\notin\Gamma_{\mathbb{S}}^F} c_i^{LS} S_i^D y_i + \sum_{ij\in\Gamma_B^C} c_{ij}^{SW}(1-w_{ij}) + \\ &\sum_{ij\in\Gamma_B^O} c_{ij}^{SW} w_{ij} + \sum_{i\in\Gamma_N^{CB}} c_i^{CB}\hat{n}_i^{CB} + \sum_{i\in\Gamma_N^{DG}} \left(c_i^{DGp}\hat{P}_i^{DG} + c_i^{DGq}\hat{Q}_i^{DG}\right) + \\ &\sum_{ij\in\Gamma_B^{TC}} c_{ij}^{TC}\hat{\delta}_{ij}^{TC} + c^{LP}\left(\sum_{ij\in\Gamma_B} w_{ij} - |\Gamma_N| + |\Gamma_N^{TS}| + |\Gamma_N^{AS}|\right) \quad (1)\end{aligned}$$

The first sum quantifies the total nonrestored load without considering the demand at the faulted section. Therefore, if $y_i = 1$, then node i is not restored and the value of the objective function increases; otherwise, if $y_i = 0$, node i is connected to the system. The second and third sums penalize the operation of the normally closed and normally open switches, respectively. The fourth sum penalizes the modification of the operational status of the CBs. Similarly, the active and reactive power redispatches of DGs are penalized in the fifth term. The sixth term penalizes the modifications of the tap position of the VRs and OLTCs. The last term calculates the number of basic loops formed in the system, i.e., the model guarantees the formation of the minimum number of temporary basic loops needed to improve the objective function. This last term works together with constraints (34)–(52) to control the topology of the network. Note that, in the formulation, it is not necessary to know what branches are in each loop, but only the number of basic loops in the system.

B. Network operation model

The operation of the system is determined by the power flow constraints (2)–(8).

$$P_i^S + P_i^{DG} + \sum_{ji\in\Gamma_B^R} P_{ji} - \sum_{ij\in\Gamma_B^R}(P_{ij} + R_{ij}I_{ij}^{SQ}) = \tilde{P}_i^D \quad (2)$$

$$\begin{aligned}Q_i^S + Q_i^{DG} + \check{Q}_i^{CB} + \sum_{ji\in\Gamma_B^R}(Q_{ji} + B_{ji}^{SH}V_i^{SQ}) \\ - \sum_{ij\in\Gamma_B^R}(Q_{ij} + X_{ij}I_{ij}^{SQ} - B_{ij}^{SH}V_i^{SQ}) = \tilde{Q}_i^D \quad (3)\end{aligned}$$

$$\forall i \in \Gamma_N^R$$

$$V_i^{SQ} - V_j^{SQ} + \delta_{ij}^{TC} + \zeta_{ij} = 2(R_{ij}P_{ij} + X_{ij}Q_{ij}) + Z_{ij}^2 I_{ij}^{SQ} \quad (4)$$

$$\check{v}_i\check{v}_j(\theta_i - \theta_j + \xi_{ij}) = X_{ij}P_{ij} - R_{ij}Q_{ij} \quad (5)$$

$$V_j^{SQ} I_{ij}^{SQ} \geq P_{ij}^2 + Q_{ij}^2 \quad (6)$$

$$|\zeta_{ij}| \leq M_{ij}^V(1 - w_{ij}) \quad (7)$$

$$|\xi_{ij}| \leq M_{ij}^\theta(1 - w_{ij}) \quad (8)$$

$$\forall ij \in \Gamma_B^R$$

Kirchhoff's current law is applied to the system in (2) and (3), which include the contributions of the DGs and CBs. The pi-circuit model is used to represent the lines of the subtransmission system. For the lines of the distribution system, it is common to consider $B_{ij}^{SH} = 0$. Kirchhoff's voltage law is applied to the system by (4)–(8). The slack variables ζ_{ij} and ξ_{ij}, limited in (7) and (8) (the calculations of the big-M parameters are shown in the Appendix), are used to eliminate constraints (4) and (5) from the model when a line is not operating ($w_{ij} = 0$). If the switch of the line is closed ($w_{ij} = 1$), then ζ_{ij} and ξ_{ij} are equal to zero, and (4) and (5) are taken into account in the formulation. The relationships between the statuses of the switches and the currents and power flows on the branches are presented in (9)–(11).

Constraint (5) is an approximation for the voltage phase angle difference in branch ij, considering that $\sin(\theta_i - \theta_j) \cong (\theta_i - \theta_j)$ and where $\check{v}_i$ and $\check{v}_j$ are estimates of the voltage magnitudes at nodes i and j, obtained by solving a power flow in the prefault state of the system. Constraint (5) must be considered when temporary loops are allowed to be formed.

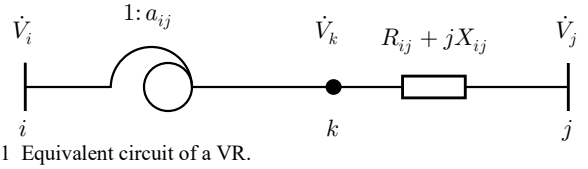

Fig. 1 Equivalent circuit of a VR.

C. Physical and operational limits of the system

Constraints (9)–(13) represent the physical and operational limits of the system.

$$0 \leq I_{ij}^{SQ} \leq \overline{I}_{ij}^{2} w_{ij} \qquad \forall ij \in \Gamma_B^R \tag{9}$$

$$|P_{ij}| \leq \overline{V}\overline{I}_{ij} w_{ij} \qquad \forall ij \in \Gamma_B^R \tag{10}$$

$$|Q_{ij}| \leq \overline{V}\overline{I}_{ij} w_{ij} \qquad \forall ij \in \Gamma_B^R \tag{11}$$

$$\underline{V}^2 \leq V_i^{SQ} \leq \overline{V}^2 \qquad \forall i \in \Gamma_N^D \tag{12}$$

$$(P_{ij})^2 + (Q_{ij})^2 \leq \left(\overline{S}_{ij}^{DS}\right)^2 \qquad \forall ij \in \Gamma_B^{DS} \tag{13}$$

Constraint (9) presents the current limit of the branches according to the state of their switches. Similarly, constraints (10) and (11) limit the active and reactive power flows on the branches of the system. The voltage limits of the demand nodes of the system are presented in (12). Finally, the quadratic constraint (13) limits the power flow through the distribution substations.

D. Load model

In this paper, the load is modeled using the voltage-dependent polynomial ZIP model [25]. Constraints (14)–(18) use the big-M formulation to calculate the value of the load according to the state of the binary variable y_i.

$$\left|\tilde{P}_i^D - P_i^D\left[\gamma_i^Z \frac{V_i^{SQ}}{(V^N)^2} + \gamma_i^I \frac{V_i}{V^N} + \gamma_i^P\right]\right| \leq M_i^P y_i \tag{14}$$

$$|\tilde{P}_i^D| \leq M_i^P (1 - y_i) \tag{15}$$

$$\left|\tilde{Q}_i^D - Q_i^D\left[\varphi_i^Z \frac{V_i^{SQ}}{(V^N)^2} + \varphi_i^I \frac{V_i}{V^N} + \varphi_i^P\right]\right| \leq M_i^Q y_i \tag{16}$$

$$\left|\tilde{Q}_i^D\right| \leq M_i^Q (1 - y_i) \tag{17}$$

$$V_i = \sqrt{\frac{\overline{V}+\underline{V}}{2}} + \frac{1}{2\sqrt{\frac{\overline{V}+\underline{V}}{2}}}\left(V_i^{SQ} - \frac{\overline{V}+\underline{V}}{2}\right) \tag{18}$$

$$\forall i \in \Gamma_N^D$$

Constraints (14) and (15) provide the values of the active power demands, while (16) and (17) provide the values of the reactive power demands (the calculations of the big-M parameters are shown in the Appendix). Note that V_i^{SQ} is available in the formulation; however, V_i needs to be calculated. Constraint (18) calculates V_i from V_i^{SQ} ($V_i = \sqrt{V_i^{SQ}}$) using a Taylor's series approximation at $V_i^{SQ} = (\overline{V} + \underline{V})/2$, in which the higher order terms are ignored. In this approximation, for $\underline{V} = 0.95$ p.u. and $\overline{V} = 1.05$ p.u., the maximum error occurs when $V_i^{SQ} = \underline{V}^2$, with a value of 0.13%.

E. Distributed generators model

The constraints related to the operation of dispatchable DGs are presented in (19)–(23).

$$(P_i^{DG})^2 + (Q_i^{DG})^2 \leq \left(\overline{S}_i^{DG}\right)^2 (1 - y_i) \tag{19}$$

$$P_i^{DG} \geq 0 \tag{20}$$

$$-P_i^{DG}\tan(\cos^{-1}(\underline{\sigma}_i)) \leq Q_i^{DG} \leq P_i^{DG}\tan(\cos^{-1}(\overline{\sigma}_i)) \tag{21}$$

$$\left|\Lambda_i^{DGp} - P_i^{DG}\right| \leq \hat{P}_i^{DG} \tag{22}$$

$$\left|\Lambda_i^{DGq} - Q_i^{DG}\right| \leq \hat{Q}_i^{DG} \tag{23}$$

$$\forall i \in \Gamma_N^{DG}$$

The quadratic constraint (19) represents the apparent power limit for the DG installed at node i. This constraint requires that a DG can only operate if its node is in-service. Constraint (20) requires that a DG only inject active power to the network. The reactive power injected by the DG installed at node i is limited in (21) as a function of the active power injected considering the capacitive and inductive power factor limits. The auxiliary constraints (22) and (23) are used to quantify the variations of the active and reactive power generations of the DGs between the prefault and the restored states of the system, which are minimized in the objective function.

F. Capacitor banks model

The operational constraints for capacitor banks are presented in (24)–(27). In this formulation, the reactive power injected by a capacitor bank is dependent on the voltage at the node in which it is installed.

$$\check{Q}_i^{CB} = \sum_{k=1}^{N_i^{CB}} Q_{i,k}^{CB} \qquad \forall i \in \Gamma_N^{CB} \tag{24}$$

$$-\overline{V}^2 B_i^{CB}(1 - h_{i,k}^{CB}) \leq Q_{i,k}^{CB} - B_i^{CB} V_i^{SQ} \leq -\underline{V}^2 B_i^{CB}(1 - h_{i,k}^{CB}) \tag{25}$$

$$B_i^{CB}\underline{V}^2 h_{i,k}^{CB} \leq Q_{i,k}^{CB} \leq B_i^{CB}\overline{V}^2 h_{i,k}^{CB} \tag{26}$$

$$\forall i \in \Gamma_N^{CB}, k \in \{1, \cdots, N_i^{CB}\}$$

$$\left|\Lambda_i^{CB} - \sum_{k=1}^{N_i^{CB}} h_{i,k}^{CB}\right| \leq \hat{n}_i^{CB} \qquad \forall i \in \Gamma_N^{CB} \tag{27}$$

Constraint (24) calculates the total reactive power injected by a CB installed at node i, $\check{Q}_i^{CB}$, as the sum of the reactive power injections of each capacitor module k, $Q_{i,k}^{CB}$. The disjunctive constraints (25) and (26) determine the individual reactive power injection of the capacitor module k at node i. Note that, if $h_{i,k}^{CB} = 0$, then $Q_{i,k}^{CB} = 0$ in (26), and V_i^{SQ} is constrained by the voltage limits of the network in (25). Otherwise, if $h_{i,k}^{CB} = 1$, then $Q_{i,k}^{CB} = B_i^{CB} V_i^{SQ}$ in (25), while the limits for $Q_{i,k}^{CB}$ are defined in (26). Finally, the auxiliary constraint (27) is used to quantify the modifications of the statuses of the CBs' modules between the prefault and the restored states of the system, which are minimized in the objective function.

G. OLTCs and voltage regulators models

In this paper, remote control is considered for the OLTCs and VRs. The operation of these devices can be modeled using discrete tap steps. However, a discrete formulation increases the complexity of the model. Thus, a new continuous formulation of the tap of VRs and OLTCs of the substations is presented. Consider an ideal transformer with a tap ratio $1:a$ in series with the transformer impedance $R_{ij} + jX_{ij}$, presented in Fig. 1. The calculation of the square of the voltage magnitude at the fictitious node k is presented in (28), while (29) defines δ_{ij}^{TC}, the difference between the square of the voltage magnitudes at nodes k and i.

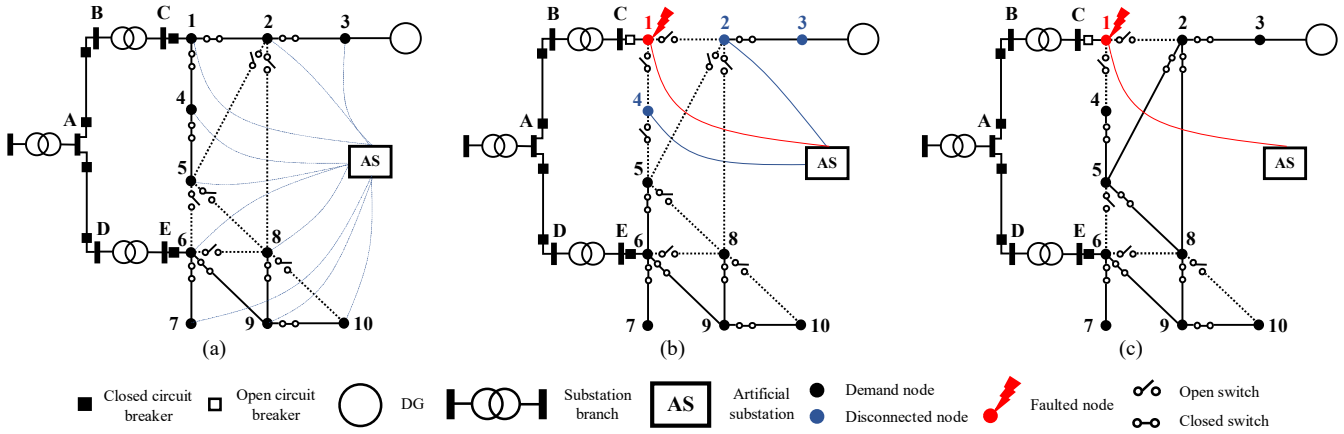

Fig. 2 Illustrative active distribution system for the network topology constraints: (a) prefault radial topology, (b) radial restoration topology, and (c) temporary closed-loop topology with connected DG operation.

$$V_k^2 = a_{ij}^2 V_i^2 \tag{28}$$

$$\delta_{ij}^{TC} = V_k^2 - V_i^2 = a_{ij}^2 V_i^2 - V_i^2 \tag{29}$$

The tap is defined as $a_{ij} = \Delta_{ij}^{TC} + 1$; thus, δ_{ij}^{TC} can be redefined as presented in (30).

$$\delta_{ij}^{TC} = \Delta_{ij}^{TC}(\Delta_{ij}^{TC} + 2)V_i^2 \tag{30}$$

Equation (31) shows how to obtain a_{ij} from δ_{ij}^{TC} and V_i.

$$a_{ij} = \frac{\sqrt{V_i^2 + \delta_{ij}^{TC}}}{V_i} \tag{31}$$

Constraint (32) is the limit for δ_{ij}^{TC}, while (33) is used to quantify the variations of the tap of VRs and OLTCs between the prefault and the restored states of the system.

$$|\delta_{ij}^{TC}| \leq \overline{\Delta}_{ij}^{TC}\left(\overline{\Delta}_{ij}^{TC} + 2\right) V_i^{SQ} \qquad \forall ij \in \Gamma_B^{TC} \tag{32}$$

$$|\Lambda_{ij}^{TC} V_i^{SQ} - \delta_{ij}^{TC} \breve{v}_i^2| \leq \hat{\delta}_{ij}^{TC} \qquad \forall ij \in \Gamma_B^{TC} \tag{33}$$

From (30), it can be verified that the terms Λ_{ij}^{TC} and δ_{ij}^{TC} of (33) include the prefault and the current values of the voltage magnitude at node i. Therefore, these terms are multiplied by V_i^{SQ} and $\breve{v}_i^2$, respectively, so that the voltage magnitudes of both terms do not influence the absolute value of the difference.

By using the proposed formulation for a typical VR or OLTC with ±16 positions for the tap, and considering $\overline{\Delta}_{ij}^{TC} = 0.1$, the maximum error that can be obtained for a_{ij} is 0.31%; in this way, it presents a good trade-off between precision and complexity.

H. Network topology constraints

By extending the concepts presented in [26], the radial operation of distribution systems can be guaranteed when (i) the number of branches in operation (including the artificial branches) is equal to $|\Gamma_N| - |\Gamma_N^{TS}| - |\Gamma_N^{AS}|$ and (ii) all of the nodes are connected through a path to exactly one subtransmission substation or to the artificial substation. Constraints (34)–(52) limit the maximum number of basic loops in the system through the parameter N^{LP}.

$$|\Gamma_N| - |\Gamma_N^{TS}| - |\Gamma_N^{AS}| \leq \sum_{ij \in \Gamma_B} w_{ij} \leq |\Gamma_N| - |\Gamma_N^{TS}| - |\Gamma_N^{AS}| + N^{LP} \tag{34}$$

In (34), if $N^{LP} = 0$, the topology of the system is required to be radial; otherwise, if $N^{LP} \geq 1$, the formulation allows the formation of up to N^{LP} temporary operational basic loops in the system.

Constraints (35)–(37) represent a sufficient condition to guarantee that each node (including demand, DG, and CB nodes) is connected to a substation if it is an in-service node.

$$\sum_{ji \in \Gamma_B} f_{ji}^e - \sum_{ij \in \Gamma_B} f_{ij}^e + g_i^e = 1 - y_i \qquad \forall i \in \Gamma_N^R \tag{35}$$

$$|f_{ij}^e| \leq |\Gamma_N| w_{ij} \qquad \forall ij \in \Gamma_B^R \tag{36}$$

$$0 \leq g_i^e \leq |\Gamma_N| \qquad \forall i \in \Gamma_N^{TS} \tag{37}$$

Constraint (35) represents an artificial flow balance in the real network that requires the existence of a path between an in-service node and a subtransmission substation, i.e., if a node is energized, $y_i = 0$, and then an artificial unity demand must be supplied by an artificial generation, g_i^e, from a subtransmission substation. Constraint (36) limits the artificial flows according to the states of the switches of the system, and (37) limits the artificial generation at the subtransmission substation nodes.

An artificial network is considered in the formulation so that the de-energized sections of the system are isolated from the main grid. This artificial network includes an artificial substation node that is connected to a node at each section of the system through an artificial branch. The set of the nodes of the real system, including the artificial substation node, is represented by Γ_N, while Γ_B includes all the branches from the real and the artificial networks.

Constraints (38)–(52) model an artificial flow in the system, including the artificial network, so that the de-energized sections of the system are isolated from the main grid.

$$\sum_{ji \in \Gamma_B} f_{ji}^f - \sum_{ij \in \Gamma_B} f_{ij}^f + g_i^f = y_i \qquad \forall i \in \Gamma_N \tag{38}$$

$$|f_{ij}^f| \leq |\Gamma_N| w_{ij} \qquad \forall ij \in \Gamma_B \tag{39}$$

$$f_{ij}^f \geq 0 \qquad \forall ij \in \Gamma_B | i \notin \Gamma_N^R \tag{40}$$

$$0 \leq g_i^f \leq |\Gamma_N| \qquad \forall i \in \Gamma_N^{AS} \tag{41}$$

$$g_i^f = 0 \qquad \forall i \in (\Gamma_N - \Gamma_N^{AS}) \tag{42}$$

$$\sum_{ji \in \Gamma_B} w_{ji} + \sum_{ij \in \Gamma_B} w_{ij} \geq 1 \qquad \forall i \in \Gamma_N^D \tag{43}$$

$$|y_i - y_j| \leq 1 - w_{ij} \qquad \forall ij \in \Gamma_B^R \tag{44}$$

$$w_{ij} \leq 1 - z_{ij} \qquad \forall ij \in \Gamma_B^O \tag{45}$$

$$w_{ij} \geq z_{ij} \qquad \forall ij \in \Gamma_B^C \tag{46}$$

$$z_{ij} \leq y_i \qquad \forall ij \in \Gamma_B^R \tag{47}$$

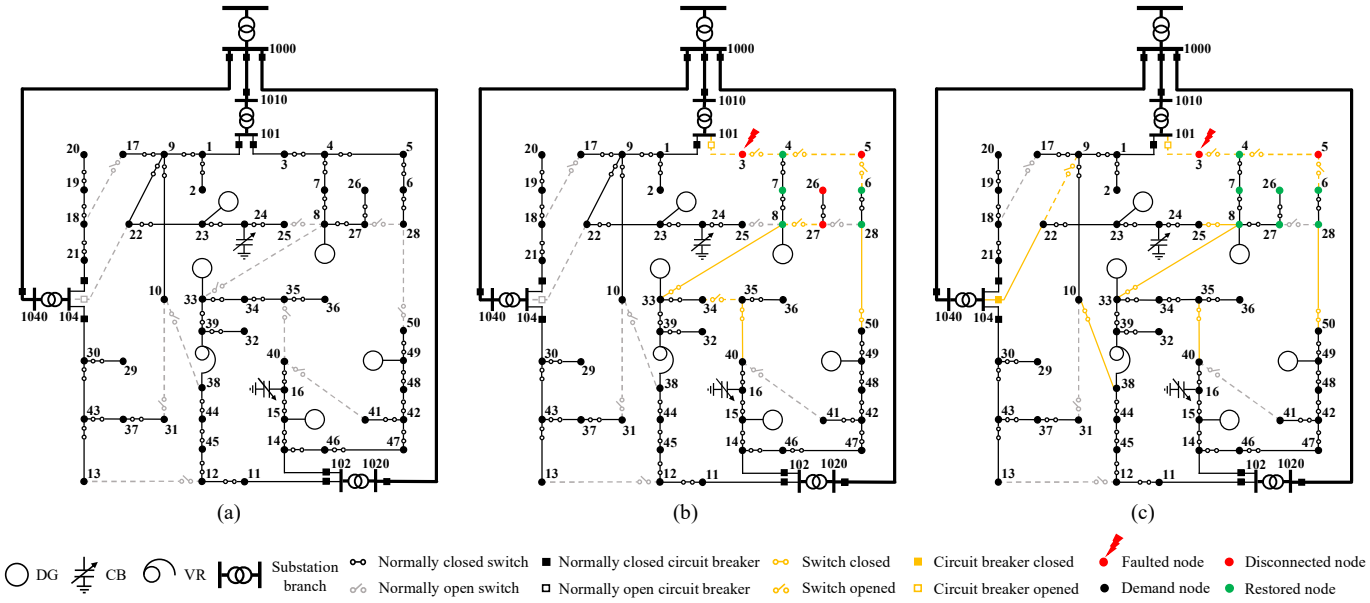

Fig. 3 (a) Prefault topology of the 53-node system and restoration topologies for Cases (b) II and (c) III.

TABLE I
FAULT SCENARIOS FOR THE 53-NODE SYSTEM

Faulted sections	Active load disconnected (kW)	Affected nodes	Opened branches
1	8828.82	2, 9, 10, 17, 22, 23, 24, 25	101-1, 9-1, 2-1
3	9639.63	4, 5, 6, 7, 8, 26, 27, 28	101-3, 4-3
11	11801.79	12, 32, 33, 34, 35, 36, 38, 39, 44, 45	102-11, 12-11
14	10540.53	15, 16, 40, 41, 42, 46, 47, 48, 49, 50	102-14, 15-14
21	3063.06	18, 19, 20	21-18, 104-21
30	5945.94	13, 29, 31, 37, 43	104-30, 29-30, 43-30
1, 21	11891.88	2, 9, 10, 17, 18, 19, 20, 22, 23, 24, 25	101-1, 9-1, 2-1, 21-18, 104-21
1, 14, 21	22432.41	2, 9, 10, 15, 16, 17, 18, 19, 20, 22, 23, 24, 25, 40, 41, 42, 46, 47, 48, 49, 50	101-1, 9-1, 2-1, 102-14, 15-14, 21-18, 104-21

$$z_{ij} \leq y_j \qquad \forall ij \in \Gamma_B^R \qquad (48)$$

$$z_{ij} \geq y_i + y_j - 1 \qquad \forall ij \in \Gamma_B^R \qquad (49)$$

$$0 \leq z_{ij} \leq 1 \qquad \forall ij \in \Gamma_B^R \qquad (50)$$

$$y_i = 0 \qquad \forall i \in (\Gamma_N^{TS} \cup \Gamma_N^{AS}) \qquad (51)$$

$$y_i = 1 \qquad \forall i \in \Gamma_N^D | \mathbb{S}_i \in \Gamma_{\mathbb{S}}^F \qquad (52)$$

Equation (38) represents the balance of the artificial flows in the system; (39) limits the artificial flow on the branches of the system according to the operational statuses of the switches; constraint (40) assumes that, for each artificial branch ij, node i represents the artificial substation and, therefore, the artificial flows can only have one direction on these branches; (41) is the limit of artificial generation at the artificial substation; and (42) fixes the artificial generation at all nodes of the system, except at the artificial substation in zero.

Constraint (43) is a fencing constraint that requires that each node be connected to at least one real or artificial branch; (44) requires that, if branch ij is connected, then the statuses of nodes i and j are the same; and constraint (45) requires that, if a branch is disconnected in the prefault state of the system, then it must remain disconnected if both nodes at its terminals are de-energized, while (46) requires that, if a branch is connected in the prefault state of the system, then it must remain connected if both nodes at its terminals are de-energized. Constraints (47)–(50) are used to calculate the auxiliary variable z_{ij} that represents the product $y_i y_j$. Constraint (51) fixes $y_i = 0$ at the subtransmission substation and at the artificial substation, and (52) fixes $y_i = 1$ at the nodes within faulted sections.

Fig. 2 (a) presents an illustrative system with ten demand nodes (numbered from 1 to 10), two distribution substations at branches B–C and D–E, an artificial substation (AS), one subtransmission substation (at node A), 20 real branches (including 16 branches in the medium-voltage system, connecting the demand nodes, two substation branches, B–C and D–E, and two branches in the subtransmission system, A–B and A–D), and ten artificial branches, connecting each demand node to the artificial substation. In the case of a fault at the section with node 1, Fig. 2 (b) illustrates the restoration topology considering $N^{LP} = 0$. Constraints (35)–(37) guarantee that each node is connected to either the subtransmission substation or to the artificial substation, while (34), (38)–(52) ensure that the resulting topology is radial. In this case, nodes 1, 2, 3, and 4 are de-energized and connected to the artificial substation.

Fig. 2 (c) illustrates the restoration topology when $N^{LP} = 1$, i.e., one loop is allowed to be formed in the system, in constraint (34). In this case, only the faulted section with node 1 is de-energized and connected to the artificial substation. Note that, in this case, constraints (35)–(37) are also satisfied.

The formulation (1)–(27) and (32)–(52) is an MISOCP model, which is convex (considering the integrality of the binary variables y_i, w_{ij}, and $h_{i,k}^{CB}$ relaxed), since the objective function (1) is linear, constraints (2)–(5), (7)–(12), (14)–(18), (20)–(27), (32)–(52) are linear, (13) and (19) are quadratic constraints, and (6) is a second-order cone constraint, therefore, it guarantees convergence to the optimal solution through optimization solvers.

TABLE II
RESULTS FOR THE RESTORATION PROBLEM CONSIDERING VOLTAGE CONTROL

Case	Faulted section	Switching operations	# of loops	Active load restored (%)	Active load not restored (kW)	De-energized nodes	Closed branches	Opened branches	Time (s)
I	1	3	0	84.69	1351.35	2	104-22, 10-38	10-9	6.64
II	3	7	0	50.47	4774.77	5, 26, 27	8-33, 35-40, 28-50	5-4, 6-5, 27-8, 35-34	8.66
III	3	9	3	75.70	2342.34	5	104-22, 8-25, 8-33, 35-40, 10-38, 28-50	5-4, 6-5, 22-9	6.98
IV	11	12	0	80.92	2252.25	38, 44	10-31, 13-12, 104-22, 8-33, 35-40, 28-50	6-5, 37-43, 22-9, 44-45, 39-38, 35-34	10.94
V	11	11	4	100.00	0.00	–	10-31, 13-12, 104-22, 8-25, 8-33, 40-41, 35-40, 10-38	37-43, 22-9, 34-33	6.05
VI	14	2	0	17.95	8648.64	15, 16, 40, 41, 42, 46, 47	28-50	48-42	4.56
VII	14	5	1	35.90	6756.75	15, 16, 40, 46, 47	104-22, 28-27, 28-50	47-42	4.03
VIII	21	3	0	100.00	0.00	–	18- 17, 104-22	22-9	6.59
IX	30	5	0	78.79	1261.26	29	10-31, 13-12, 104-22	37-43, 22-9	5.50
X	1, 21	7	0	82.58	2072.07	2, 20	18- 17, 104-22, 8-25, 10-38	10-9, 20-19, 23-22	6.70
XI	1, 21	5	1	88.64	1351.35	2	18-17, 104-22, 8-25, 10-38	10-9	7.02
XII	1, 14, 21	9	0	52.21	10720.71	2, 15, 16, 20, 40, 41, 42, 46, 47	18-17, 104-22, 8-25, 10-38, 28-50	10-9, 20-19, 24-23, 48-42	4.89
XIII	1, 14, 21	10	2	57.03	9639.63	2, 14, 15, 16, 20, 21, 40, 41, 46, 47	18-17, 104-22, 8-25, 28-27, 10-38, 28-50	10-9, 20-19, 42-41, 47-42	4.53

TABLE III
OPTIMAL OPERATION OF THE VOLTAGE CONTROL DEVICES AND DGS

Case	Number of CBs operating/$\check{Q}_i^{CB}$ (kVAr)		Tap positions VRs/OLTCs				P_i^{DG} (kW)/Q_i^{DG} (kVAr)				
	Node 16	Node 24	Branch 1010-101	Branch 1020-102	Branch 1040-104	Branch 39-38	Node 8	Node 15	Node 23	Node 33	Node 49
Base	2/635.78	2/632.05	8	9	8	8	173.00/500.00	272.00/120.00	272.00/120.00	1150.00/500.00	272.00/120.00
I	2/634.78	2/640.02	8	9	8	8	455.90/205.31	475.40/154.90	482.64/130.62	1554.92/687.19	458.06/200.46
II	4/1118.61	4/1088.02	–5	–1	–5	–1	451.11/215.64	479.21/142.68	486.10/117.08	1537.07/726.24	458.03/200.51
III	4/1132.81	4/1106.46	–1	1	–4	–1	474.14/158.72	473.54/160.50	470.76/168.48	1592.25/595.59	464.88/184.09
IV	4/1119.75	2/556.02	–2	–2	–4	8	453.71/210.12	480.07/139.77	485.39/120.00	1538.35/723.51	456.53/203.92
V	4/1101.76	4/1127.53	–2	–3	–2	1	462.75/189.37	475.40/154.90	479.76/140.81	1556.49/683.62	463.10/188.51
VI	2/0.00	2/632.57	8	9	8	8	456.70/203.54	0.00/0.00	477.28/149.01	1360.00/–1020.00	453.34/210.92
VII	2/0.00	2/548.90	–1	9	–5	12	454.71/207.94	0.00/0.00	485.39/120.00	1539.01/722.12	452.85/211.95
VIII	2/636.77	2/646.57	8	9	8	8	456.43/204.15	474.55/157.49	485.39/120.00	1554.26/688.68	457.38/202.00
IX	2/635.12	2/648.58	8	9	8	8	456.49/204.01	474.88/156.48	485.39/120.00	1554.78/687.50	457.72/201.22
X	2/634.78	2/636.33	8	9	8	8	465.77/181.82	475.40/154.90	474.20/158.52	1554.92/687.19	458.06/200.46
XI	4/1115.83	4/1135.63	–1	–2	–3	1	470.00/170.58	483.97/125.61	474.76/156.86	1539.65/720.76	459.64/196.80
XII	2/0.00	4/1102.68	–4	9	–3	11	477.12/149.52	0.00/0.00	457.06/202.73	1537.48/725.37	458.60/199.22
XIII	2/0.00	4/1118.22	–2	9	–4	11	467.83/176.45	0.00/0.00	467.80/176.52	1537.48/725.37	460.33/195.17

III. TESTS AND RESULTS

The performance and robustness of the proposed model are tested and analyzed using a modified version of the 53-node distribution system presented in [20]. Fig. 3 (a) shows the prefault topology of the system, which has 50 load nodes. The subtransmission system operates at a nominal voltage of 138 kV, and the subtransmission substation at node 1000 is connected to the distribution substations (1010-101, 1020-102, and 1040-104) through branches 1000-1010, 1000-1020, and 1000-1040. The nominal voltage of the distribution system is 13.8 kV, while the minimum and maximum voltage limits are 0.95 p.u. and 1.05 p.u., respectively. In the distribution system, each branch has an automatic switch; therefore, each node represents a section of the network. A VR with $\overline{\Delta}_{ij}^{TC} = 0.1$ and ±16 positions for the tap is installed at branch 38-39. The transformers at the distribution substations are equipped with OLTCs, with $\overline{\Delta}_{ij}^{TC} = 0.1$ and ±16 positions for the taps. Two 1200 kVAr CBs with $N_i^{CB} = 4$ are installed at nodes 16 and 24. Five dispatchable DGs, with $\overline{S}_i^{DG}$ of 500 kVA, 500 kVA, 500 kVA, 1700 kVA, and 500 kVA and $\underline{\sigma}_i = \overline{\sigma}_i = 0.8$, are installed at nodes 8, 15, 23, 33, and 49, respectively. The costs considered in the objective function are $c_i^{LS} = 10$ US$/kVA, $c_{ij}^{SW} = 150$ US$, $c_i^{CB} = 10$ US$, $c_i^{DGp} = 0.01$ US$/kW, $c_i^{DGq} = 0.01$ US$/kVAr, $c_{ij}^{TC} = 10$ US$, and $c^{LP} = 10$ US$. The complete data for this system are available in [27].

The optimization model was implemented in AMPL [28] and solved with the solver CPLEX v12.9 [29]. The numerical experiments have been conducted on a computer with a 3.2 GHz Intel® Core™ i7-8700 processor and 32 GB of RAM.

A. Fault scenarios

The proposed model is tested considering single permanent faults at the sections of nodes 1, 3, 11, 14, 21, and 30. Also, scenarios with multiple permanent faults at the sections of nodes {1, 21} and {1, 14, 21} are considered. These scenarios are the ones that lead to the higher values of disconnected load after the fault and occur at the beginning of the feeders, therefore it is expected that they are among the hardest scenarios to be solved. For these fault scenarios, Table I presents the nodes of the faulted sections, the total isolated active load that can be restored (without taking into account the demand at the faulted sections), the nodes affected by the faults that are candidates to be restored, and the switches opened to isolate the faulted sections, which must remain open until the maintenance crews carry out the necessary repairs.

B. Obtained results

Table II presents thirteen cases with the optimal topologies for the restoration problem in each one of the eight single-fault and multiple-fault scenarios presented in Table I, considering voltage control. In these thirteen cases, eight (I, II, IV, VI, VIII, IX, X, and XII) represent radial topologies, one for each fault scenario, and five cases (III, V, VII, XI, and XIII) present temporary closed-loop topologies for the fault scenarios in which this topological condition allows more load to be restored.

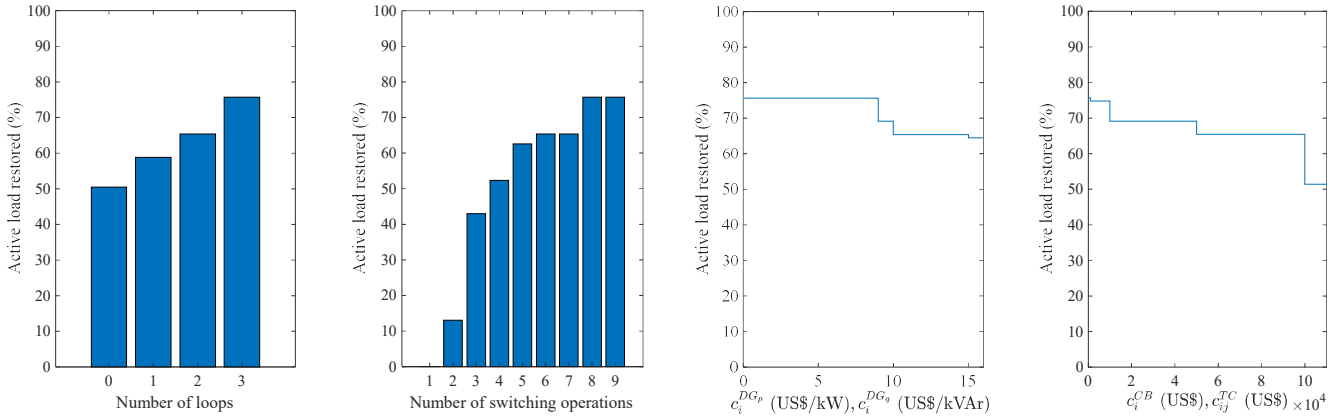

(a) (b) (c) (d)

Fig. 4 Sensitivity analysis in the percentage of the active load restored for a fault at section 3 according to the (a) maximum number of loops allowed to be formed, (b) maximum number of switching operations, (c) DGs' operation costs, (d) voltage control devices' operation costs.

TABLE IV
RESULTS WITHOUT CONSIDERING VOLTAGE CONTROL

Case	Faulted section	Switching operations	# of loops	Active load restored (%)	Active load not restored (kW)	De-energized nodes	Time (s)
I	1	3	0	84.69	1351.35	2	7.11
II	3	7	0	43.93	5405.40	5, 6, 26, 27	8.88
III	3	6	1	51.40	4684.68	5, 6, 26, 28	11.91
IV	11	16	0	69.47	3603.60	34, 36, 38, 44	13.19
V	11	13	5	86.26	1621.62	12	8.30
VI	14	2	0	17.95	8648.64	15, 16, 40, 41, 42, 46, 47	4.50
VII	14	6	3	28.21	7567.56	15, 16, 40, 41, 46, 47	4.88
VIII	21	3	0	100.00	0.00	–	5.20
IX	30	5	0	78.79	1261.26	29	5.91
X	1, 21	7	0	82.58	2072.07	2, 20	6.48
XI	1, 21	7	0	82.58	2072.07	2, 20	7.95
XII	1, 14, 21	9	0	49.00	11441.43	2, 15, 16, 20, 40, 41, 42, 46, 47, 48	4.58
XIII	1, 14, 21	10	2	51.41	10900.89	2, 15, 16, 19, 20, 40, 41, 46, 47	4.77

For each case, Table II presents the nodes in the faulted sections, the number of switching operations required to restore the load (not accounting for the operations to isolate the faulted sections, presented in Table I), the number of basic loops formed in the network, the percentage of the active load restored (not accounting for the load in the sections directly affected by the fault), the active load not restored, the de-energized nodes that are isolated from the system, the branches connected to the system, the branches disconnected from the system, and the computational times to solve the problem.

The results presented in Table II indicate that, in some cases, by considering the temporary closed-loop operation during the restorative state, it is possible to restore more load. In Case III, for example, it is possible to restore 75.70% of the load by allowing a temporary loop formation in the system, which represents 25.23% more load restored in comparison to Case II, which considers a radial configuration. Fig. 3 (b) illustrates the radial restoration topology of the system for Case II, while Fig. 3 (c) shows the restoration topology with three basic loops for Case III. In Cases V, VII, XI, and XIII, it is also possible to verify improvements of 19.08%, 17.95%, 6.06%, and 4.82%, respectively, in the active load restored of the solutions when a temporary closed-loop operation is allowed when compared to the respective radial restoration topologies.

Table III summarizes the adjustment of the voltage control devices and the dispatch of the DGs in each case and in the Base Case, before the occurrence of the fault. By analyzing Table III, it is possible to verify a tendency of the model to provide restoration plans that reduce the voltage magnitudes in the system through the operation of the OLTCs and VRs, so that the load, which is modeled using a voltage-dependent formulation, decreases. It can also be verified that the DGs are redispatched in some cases so that more load is reconnected. For all the cases, the minimum voltage magnitude obtained in the system was 0.95 p.u.

Table IV shows the results for Cases I–XIII, without considering voltage control in the restoration problem, i.e., the number of CBs connected to nodes 16 and 24 and the positions of the taps of VRs and OLTCs are fixed at the values presented for the Base Case in Table III. For Cases I, VI, VIII, IX, and X, the values for the active load restored are the same as the ones presented in Table II for the respective cases. For the other eight cases, reductions in the range of 3.21%–24.30% can be noticed in the active load restored when voltage control is not considered in the restoration problem, for situations considering both radial and temporary closed-loop topologies.

Fig. 4 shows the influence of the change of some parameters of the model in the solutions of the restoration problem for the fault scenario in section 3. Four cases were considered, and in each one of them, all other parameters were maintained constant with the values presented at the beginning of this section. First, Fig. 4 (a) shows that by not allowing the formation of loops, 50.47% of the active load is restored, as presented in Case II in Table II. By increasing the number of loops allowed to be formed, more load can be restored, up to a maximum of 75.70% (the same solution of Case III in Table II). In Fig. 4 (b), the solutions are obtained considering different values for the maximum number of switching operations allowed. Note that when only one switching operation is allowed, no load can be restored; by allowing two operations 13.08% of the active load is restored; and by allowing eight switching operations, 75.70% of the active load is restored, while four loops are formed in the network. By allowing nine switching operations, the active load restored does not increase, but the number of loops formed in the network is reduced to three (the solution is the same one of Case III in Table II). Fig. 4 (c) shows the influence of the DGs' operational costs on the active load restored. When c_i^{DGp} and c_i^{DGq} are equal to 0.1 US$/kW and 0.1 US$/kVAr or less, 75.70% of the active load is restored, leading to the solution of

Case III presented in Table II, and this value is reduced to 64.49% as c_i^{DGp} and c_i^{DGq} are increased to 16 US$/kW and 16 US$/kVAr. In this case, the dispatches of the DGs remain with the values presented for the Base Case in Table III. Finally, Fig. 4 (d) shows the influence of the operation cost of CBs, VRs, and substations' OLTCs in the restored load. Note that when $c_i^{CB} = c_{ij}^{TC} = 10$ US$, the active load restored is 75.70% as for Case III in Table II. When c_i^{CB} and c_{ij}^{TC} are increased to 100,000.00 US$ or more, the active load restored is reduced to 51.40%, as presented in Case III in Table IV.

The results presented in Fig. 4 indicate that, for a fault in section 3, the maximum number of switching operations has the greatest impact in the value of the active load restored, followed by the number of loops allowed to be formed in the system. Then, it can be observed that the voltage control devices have a greater impact on the active load restored than the redispatch of the DGs. This information can be useful to the system planner for deciding about future investments in the network.

C. Discussion of the results

By analyzing the results, it is possible to verify that the temporary closed-loop operation allows more load to be restored in some fault scenarios. Besides that, it does not require the installation of new devices in the network, so it can be used to easily improve the reliability indexes of the system. The consideration of voltage control devices and DGs in the restoration problem allows the obtention of better restoration plans, with more load restored and with better quality in the service. It can also be verified that the model is flexible since it is possible to consider single-fault and multiple-fault scenarios in the restoration problem. Besides that, it is possible to take into account preferential loads and differentiate between automatic and manual switches by choosing adequate costs in the objective function. It should be noted that, as in [20], the model provides solutions in which some sections can be disconnected from the network during the restorative operation state.

All results were verified using a backward/forward sweep power flow algorithm [30]. The power flow analysis indicated, for all the solutions, that all the operational constraints of the system were met, therefore demonstrating the precision of the formulation.

Finally, the computational times required to solve all the cases are in the range of 4.03 s to 13.19 s, which are adequate for the timeframe of the restoration problem.

IV. Conclusion

This paper presented a new mixed-integer second-order cone programming formulation to the problem of service restoration in distribution systems, considering voltage control devices, distributed generators, and temporary closed-loop operation in the restorative state. The model accounted for an accurate ac representation of the network operation, considering a voltage-dependent model for the loads. Besides that, the constraints allow controlling the formation of loops in the network, providing flexibility to the solutions.

The results indicate that, by allowing the formation of temporary loops in the network during the restorative state and performing the simultaneous control of voltage devices, it is possible to obtain solutions with more load restored when compared to the radial solutions provided by the traditional approach. It was also verified that the voltage control devices reduce the voltage magnitudes in the system in order to decrease the load, allowing for more efficient restoration schemes.

The proposed strategy of a temporary closed-loop operation, together with the optimal adjustment of voltage control devices in active distribution networks during the restorative state, is an alternative for improving the reliability indexes and could be used to reduce future investments in the system.

Appendix

In this appendix, we present the calculation of the big-M parameters used in constraints (7), (8), and (14)–(17). Note that, the values of these parameters should be large enough, so that no solution is eliminated from the feasible region of the problem, but should not be unnecessarily large so that the computational effort to solve the problem is not high. All the big-M parameters used for the 53-node distribution system are available in [27].

A. Calculation of M_{ij}^V

Equations (53) and (54) provide the values for M_{ij}^V, used in (7), for branches without and with OLTCs or VRs, respectively.

$$M_{ij}^V = \overline{V}^2 - \underline{V}^2 \qquad \forall ij \in \Gamma_B^R | ij \notin \Gamma_B^{TC} \tag{53}$$

$$M_{ij}^V = \overline{V}^2 - \underline{V}^2 + \overline{\Delta}_{ij}^{TC}\left(\overline{\Delta}_{ij}^{TC} + 2\right)\overline{V}^2 \qquad \forall ij \in \Gamma_B^{TC} \tag{54}$$

For the tests presented in this paper, with $\underline{V} = 0.95$ p.u., $\overline{V} = 1.05$ p.u., and $\overline{\Delta}_{ij}^{TC} = 0.1$ for OLTCs and VRs, $M_{ij}^V = 0.20$ for branches without OLTCs and VRs and $M_{ij}^V = 0.431525$ for branches with OLTCs and VRs.

B. Calculation of M_{ij}^θ

The parameter M_{ij}^θ, that appears in (8), is the maximum voltage phase angle difference between the terminal nodes of branch ij when it is open. Note that, M_{ij}^θ depends on the maximum value for the sum of the maximum voltage phase angle differences between the terminal nodes of the branches that form a loop with branch ij.

By analyzing (5), it is possible to verify that the maximum value of the voltage phase angle difference between the terminal nodes of branch ij when it is operating, $\overline{\theta}_{ij}$, occurs when $(X_{ij}P_{ij} + R_{ij}Q_{ij})/\underline{V}^2$ is maximum. The model (55) and (56) is used to calculate the maximum value of $(X_{ij}P_{ij} + R_{ij}Q_{ij})/\underline{V}^2$ considering (6) and the operational limits of the network, (9) and (12).

$$\text{maximize}\, \mathcal{T} = \sum_{ij \in \Gamma_B^R} \frac{X_{ij}P_{ij} + R_{ij}Q_{ij}}{\underline{V}^2} \tag{55}$$

subject to:

$$P_{ij}^2 + Q_{ij}^2 \leq \overline{V}^2 \overline{I}_{ij}^2 \qquad \forall ij \in \Gamma_B^R \tag{56}$$

The objective function $\mathcal{T}$, shown in (55), is obtained from (5). Constraint (56) is the power flow limit for the branches. Let P_{ij}^* and Q_{ij}^* be the solution of (55) and (56), then $\overline{\theta}_{ij} = (X_{ij}P_{ij}^* + R_{ij}Q_{ij}^*)/\underline{V}^2$.

Initial step: Calculate $\overline{\theta}_{ij}$ $\forall ij \in \Gamma_B^R$ using (55) and (56). Let $\overline{\theta}_{ji} \leftarrow \overline{\theta}_{ij}$ $\forall ij \in \Gamma_B^R$.
For all $ij \in \Gamma_B^R$, excluding the branches that cannot form loops with other branches:
    Fix $x_{ij} \leftarrow 0$
    Fix $x_{ji} \leftarrow 0$
    For all $k \in \Gamma_N^{R*}$:
        Let $b_k \leftarrow 0$
    End
    Let $b_i \leftarrow 1$
    Let $b_j \leftarrow -1$
    Solve model (57)–(63). The value of $\mathcal{D}$ is determined.
    Let $M_{ij}^{\theta} \leftarrow \mathcal{D}$
    Unfix x_{ij}
    Unfix x_{ji}
End

Fig. 5 Pseudocode for the algorithm that calculates M_{ij}^{θ}.

The value of M_{ij}^{θ} is the maximum value of the sum of $\overline{\theta}_{ij}$ on a path connecting nodes i and j when branch ij is disconnected from the system. Therefore, to obtain the value of M_{ij}^{θ} for a branch ij, it is necessary to remove branch ij and then solve the longest path problem considering that $\overline{\theta}_{ij}$ is the length of branch ij. The model (57)–(63) is used to obtain the longest path (considering that $\overline{\theta}_{ij}$ is the length of branch ij) between two nodes of the system (which can be represented as a graph) [31].

$$\text{maximize}\, \mathcal{D} = \sum_{ij \in \Gamma_B^{R*}} \overline{\theta}_{ij} x_{ij} \tag{57}$$

subject to:

$$\sum_{ji \in \Gamma_B^{R*}} x_{ji} - \sum_{ij \in \Gamma_B^{R*}} x_{ij} + b_i = 0 \qquad \forall i \in \Gamma_N^{R*} \tag{58}$$

$$\sum_{ij \in \Gamma_B^{R*}} x_{ij} \leq 1 \qquad \forall i \in \Gamma_N^{R*} \tag{59}$$

$$\sum_{ji \in \Gamma_B^{R*}} x_{ji} \leq 1 \qquad \forall i \in \Gamma_N^{R*} \tag{60}$$

$$t_j \geq t_i + 1 - (|\Gamma_N^{R*}| - 1)(1 - x_{ij}) \qquad \forall ij \in \Gamma_B^{R*} \tag{61}$$

$$t_i \geq 0 \qquad \forall i \in \Gamma_N^{R*} \tag{62}$$

$$x_{ij} + x_{ji} \leq 1 \qquad \forall ij \in \Gamma_B^{R*} | i > j \tag{63}$$

In (57)–(63), the set Γ_B^{R*} includes the branches of the system with duplicated indices ij and ji, excluding the branches that cannot form loops with other branches, and the set Γ_N^{R*} includes all nodes of the system, except the ones that do not belong to a loop. The parameter b_i is equal to 1 (inflow) at a terminal node of the branch that was removed, –1 (outflow) at the other terminal node, and is equal to zero at the other nodes. The integer-valued continuous variable t_i indicates the order in which the nodes are visited, and is used in the sub-tour elimination constraint, as proposed by [32]. The binary variable x_{ij} is equal to 1 if branch ij is part of the path and is equal to 0 otherwise. Also, $\overline{\theta}_{ji} = \overline{\theta}_{ij}$ $\forall ij \in \Gamma_B^R$.

The objective function $\mathcal{D}$, shown in (57), maximizes the length of the path between two nodes. Note that, since each branch is duplicated, the index ij represents a branch with direction from i to j (outflow from node i), while ji represents a branch with direction from j to i (inflow to node i). Constraint (58) requires that the inflow is equal to the outflow at each node. Constraint (59) requires that each node can have a maximum of one outflow branch active, while (60) requires that each node can have a maximum of one inflow branch active. Constraints (61) and (62) are used to avoid the formation of sub-tours [32]. Constraint (63) requires that a maximum of one direction is chosen for each branch.

Fig. 5 shows the pseudocode of the algorithm used to obtain M_{ij}^{θ} for each branch. Initially, $\overline{\theta}_{ij}$ is calculated for all branches using (55) and (56). Then, at each step, branch ij is removed from the system (x_{ij} and x_{ji} are fixed at zero), b_i is set to zero at all nodes, and then fixed in 1 at node i and in –1 at node j. Model (57)–(63) is then solved, and the value of M_{ij}^{θ} is defined as $\mathcal{D}$. Finally, branch ij is reincorporated to the system (x_{ij} and x_{ji} are unfixed). This process is repeated for all branches of the system. For the branches that cannot form loops $M_{ij}^{\theta} = 0$.

For the system used in the tests, the values for M_{ij}^{θ} are within the range of 0.4621 p.u. and 0.8290 p.u., excluding the branches that cannot form loops with other branches.

C. Calculation of M_i^P and M_i^Q

Equations (64) and (65) provide the values for M_i^P and M_i^Q, respectively, used in (14)–(17).

$$M_i^P = P_i^D \left[\gamma_i^Z \frac{\overline{V}^2}{(V^N)^2} + \gamma_i^I \frac{\overline{V}}{V^N} + \gamma_i^P \right] \qquad \forall i \in \Gamma_N^D \tag{64}$$

$$M_i^Q = Q_i^D \left[\varphi_i^Z \frac{\overline{V}^2}{(V^N)^2} + \varphi_i^I \frac{\overline{V}}{V^N} + \varphi_i^P \right] \qquad \forall i \in \Gamma_N^D \tag{65}$$

Note that, these values are obtained when the maximum voltage magnitude is considered at each node.

REFERENCES

[1] S. Ćurčić, C. S. Özveren, L. Crowe, and P. K. L. Lo, "Electric power distribution network restoration: a survey of papers and a review of the restoration problem," *Electr. Power Syst. Res.*, vol. 35, no. 2, pp. 73–86, Nov. 1995.

[2] A. Zidan *et al.*, "Fault detection, isolation, and service restoration in distribution systems: state-of-the-art and future trends," *IEEE Trans. Smart Grid*, vol. 8, no. 5, pp. 2170–2185, Sep. 2017.

[3] T. Gönen, *Electric power distribution engineering*, 3rd ed. Boca Raton: CRC Press, 2014.

[4] D. Ritter, J. F. Franco, and R. Romero, "Analysis of the radial operation of distribution systems considering operation with minimal losses," *Int. J. Electr. Power Energy Syst.*, vol. 67, pp. 453–461, May 2015.

[5] R. A. V. Peralta, J. B. Leite, and J. R. S. Mantovani, "Automatic restoration of large-scale distribution networks with distributed generators, voltage control devices and heating loads," *Electr. Power Syst. Res.*, vol. 176, pp. 1–11, Nov. 2019.

[6] J. S. Wu, K. L. Tomsovic, and C. S. Chen, "A heuristic search approach to feeder switching operations for overload, faults, unbalanced flow and maintenance," *IEEE Trans. Power Deliv.*, vol. 6, no. 4, pp. 1579–1585, Oct. 1991.

[7] C.-H. Lee and C.-M. Huang, "Analysis of load transfer on radial distribution systems with tie lines," *Eur. Trans. Electr. Power*, vol. 17, no. 3, pp. 268–284, May 2007.

[8] T. H. Chen, W. T. Huang, J. C. Gu, G. C. Pu, Y. F. Hsu, and T. Y. Guo, "Feasibility study of upgrading primary feeders from radial and open-loop to normally closed-loop arrangement," *IEEE Trans. Power Syst.*, vol. 19, no. 3, pp. 1308–1316, Aug. 2004.

[9] N. Jenkins, R. Allan, P. Crossley, D. Kirschen, and G. Strbac, *Embedded generation*, 1st ed. Stevenage: IET, 2000.

[10] Y. Li, J. Xiao, C. Chen, Y. Tan, and Y. Cao, "Service restoration model with mixed-integer second-order cone programming for distribution network with distributed generations," *IEEE Trans. Smart Grid*, vol. 10, no. 4, pp. 4138–4150, Jul. 2019.

[11] T. Senjyu, Y. Miyazato, A. Yona, N. Urasaki, and T. Funabashi, "Optimal distribution voltage control and coordination with distributed generation," *IEEE Trans. Power Deliv.*, vol. 23, no. 2, pp. 1236–1242, Apr. 2008.

[12] A. Majumdar, Y. P. Agalgaonkar, B. C. Pal, and R. Gottschalg, "Centralized volt–var optimization strategy considering malicious attack on distributed energy resources control," *IEEE Trans. Sustain. Energy*, vol. 9, no. 1, pp. 148–156, Jan. 2018.
[13] R. W. Uluski, "VVC in the smart grid era," in *IEEE PES General Meeting*, 2010, pp. 1–7.
[14] H. Sekhavatmanesh and R. Cherkaoui, "Analytical approach for active distribution network restoration including optimal voltage regulation," *IEEE Trans. Power Syst.*, vol. 34, no. 3, pp. 1716–1728, May 2019.
[15] S. Riahinia, A. Abbaspour, M. Moeini-Aghtaie, and S. Khalili, "Load service restoration in active distribution network based on stochastic approach," *IET Gener. Transm. Distrib.*, vol. 12, no. 12, pp. 3028–3036, Jul. 2018.
[16] D. S. Sanches, J. B. A. London, and A. C. B. Delbem, "Multi-objective evolutionary algorithm for single and multiple fault service restoration in large-scale distribution systems," *Electr. Power Syst. Res.*, vol. 110, pp. 144–153, May 2014.
[17] L. T. Marques, A. C. B. Delbem, and J. B. London, "Service restoration with prioritization of customers and switches and determination of switching sequence," *IEEE Trans. Smart Grid*, vol. 9, no. 3, pp. 2359–2370, May 2018.
[18] K. N. Miu, H.-D. Chiang, and R. J. McNulty, "Multi-tier service restoration through network reconfiguration and capacitor control for large-scale radial distribution networks," *IEEE Trans. Power Syst.*, vol. 15, no. 3, pp. 1001–1007, Aug. 2000.
[19] F. Glover and G. A. Kochenberger, *Handbook of metaheuristics*. Dordrecht: Kluwer Academic Publishers, 2003.
[20] R. Romero, J. F. Franco, F. B. Leão, M. J. Rider, and E. S. de Souza, "A new mathematical model for the restoration problem in balanced radial distribution systems," *IEEE Trans. Power Syst.*, vol. 31, no. 2, pp. 1259–1268, Mar. 2016.
[21] B. Chen, C. Chen, J. Wang, and K. L. Butler-Purry, "Sequential service restoration for unbalanced distribution systems and microgrids," *IEEE Trans. Power Syst.*, vol. 33, no. 2, pp. 1507–1520, Mar. 2018.
[22] B. Chen, C. Chen, J. Wang, and K. L. Butler-Purry, "Multi-time step service restoration for advanced distribution systems and microgrids," *IEEE Trans. Smart Grid*, vol. 9, no. 6, pp. 6793–6805, Nov. 2018.
[23] K. S. A. Sedzro, A. J. Lamadrid, and L. F. Zuluaga, "Allocation of resources using a microgrid formation approach for resilient electric grids," *IEEE Trans. Power Syst.*, vol. 33, no. 3, pp. 2633–2643, May 2018.
[24] G. W. Stagg and A. H. El-Abiad, *Computer methods in power system analysis*, 1st ed. New York: McGraw-Hill, 1968.
[25] L. M. Hajagos and B. Danai, "Laboratory measurements and models of modern loads and their effect on voltage stability studies," *IEEE Trans. Power Syst.*, vol. 13, no. 2, pp. 584–592, May 1998.
[26] M. Lavorato, J. F. Franco, M. J. Rider, and R. Romero, "Imposing radiality constraints in distribution system optimization problems," *IEEE Trans. Power Syst.*, vol. 27, no. 1, pp. 172–180, Feb. 2012.
[27] "LaPSEE power system test cases repository," 2020. [Online]. Available: http://www.feis.unesp.br/#!/lapsee. [Accessed: 03-Nov-2020].
[28] R. Fourer, D. M. Gay, and B. W. Kernighan, *AMPL: a modeling language for mathematical programming*, 2nd ed. Duxbury, MA, USA: Thomson, 2003.
[29] IBM, "IBM ILOG CPLEX optimization studio v12.9.0 documentation," 2019. [Online]. Available: https://www.ibm.com/support/knowledgecenter/en/SSSA5P_12.9.0/ilog.odms.studio.help/Optimization_Studio/topics/COS_home.html. [Accessed: 15-Jun-2020].
[30] D. Shirmohammadi, H. W. Hong, A. Semlyen, and G. X. Luo, "A compensation-based power flow method for weakly meshed distribution and transmission networks," *IEEE Trans. Power Syst.*, vol. 3, no. 2, pp. 753–762, May 1988.
[31] L. Taccari, "Integer programming formulations for the elementary shortest path problem," *Eur. J. Oper. Res.*, vol. 252, no. 1, pp. 122–130, Jul. 2016.
[32] C. E. Miller, A. W. Tucker, and R. A. Zemlin, "Integer programming formulation of traveling salesman problems," *J. ACM*, vol. 7, no. 4, pp. 326–329, Oct. 1960.

Renzo Vargas (S'15–M'20) received the B.Sc. degree in electrical engineering from the National University Engineering, Lima, Peru, in 2012, and the M.Sc. and Ph.D. degrees in electrical engineering from the São Paulo State University (UNESP), Ilha Solteira, Brazil, in 2015 and 2019, respectively. Currently, he is carrying out postdoctoral research with the UNESP.

His research interests include the development of methodologies for the optimization and planning of electrical power systems.

Leonardo H. Macedo (S'14–M'18) received the B.Sc., M.Sc., and Ph.D. degrees from the São Paulo State University, São Paulo, Brazil, in 2012, 2015, and 2019, respectively, where he is currently a postdoctoral researcher.

His current research interests include the development of methods for the optimization, planning, and control of electrical power systems.

Juan M. Home-Ortiz received the B.Sc. and M.Sc. degrees in electrical engineering from the Universidad Tecnológica de Pereira, Colombia, in 2011 and 2014, respectively, and the Ph.D. degree in electrical engineering from the São Paulo State University (UNESP), Ilha Solteira, Brazil, in 2019. Currently, he is carrying out postdoctoral research with the UNESP.

His research interests include the development of methodologies for the optimization, planning, and control, of electrical power systems.

José Roberto Sanches Mantovani (M'06) received the B.Sc. degree from the São Paulo State University (UNESP), Ilha Solteira, Brazil, in 1981, and the M.Sc. and Ph.D. degrees from the University of Campinas, Campinas, Brazil, in 1987 and 1995, respectively, all in electrical engineering. He is currently a professor with the Department of Electrical Engineering, UNESP.

His research interests include the development of methodologies for the optimization, planning, and control of electrical power systems, and applications of artificial intelligence in power systems.

Rubén Romero (M'93–SM'08) received the B.Sc. and P.E. degrees from the National University of Engineering, Lima, Peru, in 1978 and 1984, respectively. He received the M.Sc. and Ph.D. degrees from the University of Campinas, Campinas, Brazil, in 1990 and 1993, respectively. He is currently a professor of electrical engineering at the São Paulo State University, Ilha Solteira, Brazil.

His research interests include methods for the optimization, planning, and control of electrical power systems, applications of artificial intelligence in power systems, and operations research.